

1-1-2012

## A two-stage approach for measuring vascular water exchange and arterial transit time by diffusion-weighted perfusion MRI

Keith S. St. Lawrence  
*Lawson Health Research Institute, kstlawr@uwo.ca*

Daron Owen  
*Ottawa Hospital Research Institute*

Danny J.J. Wang  
*University of California, Los Angeles*

Follow this and additional works at: <https://ir.lib.uwo.ca/paedpub>

---

### Citation of this paper:

St. Lawrence, Keith S.; Owen, Daron; and Wang, Danny J.J., "A two-stage approach for measuring vascular water exchange and arterial transit time by diffusion-weighted perfusion MRI" (2012). *Paediatrics Publications*. 1510.

<https://ir.lib.uwo.ca/paedpub/1510>

# A Two-Stage Approach for Measuring Vascular Water Exchange and Arterial Transit Time by Diffusion-Weighted Perfusion MRI

Keith S. St. Lawrence,<sup>1\*</sup> Daron Owen,<sup>2</sup> and Danny J. J. Wang<sup>3</sup>

**Changes in the exchange rate of water across the blood-brain barrier, denoted  $k_w$ , may indicate blood-brain barrier dysfunction before the leakage of large-molecule contrast agents is observable. A previously proposed approach for measuring  $k_w$  is to use diffusion-weighted arterial spin labeling to measure the vascular and tissue fractions of labeled water, because the vascular-to-tissue ratio is related to  $k_w$ . However, the accuracy of diffusion-weighted arterial spin labeling is affected by arterial blood contributions and the arterial transit time ( $\tau_a$ ). To address these issues, a two-stage method is proposed that uses combinations of diffusion-weighted gradient strengths and post-labeling delays to measure both  $\tau_a$  and  $k_w$ . The feasibility of this method was assessed by acquiring diffusion-weighted arterial spin labeling data from seven healthy volunteers. Repeat measurements and Monte Carlo simulations were conducted to determine the precision and accuracy of the  $k_w$  estimates. Average grey and white matter  $k_w$  values were  $110 \pm 18$  and  $126 \pm 18 \text{ min}^{-1}$ , respectively, which compare favorably to blood-brain barrier permeability measurements obtained with positron emission tomography. The intrasubject coefficient of variation was  $26\% \pm 23\%$  in grey matter and  $21\% \pm 17\%$  in white matter, indicating that reproducible  $k_w$  measurements can be obtained. *Magn Reson Med* 67:1275–1284, 2012. © 2011 Wiley Periodicals, Inc.**

Through the formation of tight junctions joining the endothelial cells of capillaries in the brain, the blood-brain barrier (BBB) acts to restrict and regulate the exchange of substances between the general circulation and the central nervous system (1). As such, the integrity of the BBB is critical to neuronal health, because it protects the brain from toxins, facilitates nutrient transport, and maintains ion balance. Increasing evidence suggests that BBB dysfunction is a contributing factor to a number of serious neurological diseases such as multiple sclerosis, stroke, brain tumors, central nervous system infection, and Alzheimer's disease (2). The most common biochemical assay of BBB permeability is the cerebrospinal fluid/

serum albumin ratio, which requires lumbar puncture and provides no information regarding regional BBB changes. Dynamic contrast-enhanced MRI using intravenous injection of gadolinium (Gd)-based contrast agents (e.g., Gd-DTPA) has been the most widely applied method for imaging BBB permeability in clinical settings (3). The leakage rate of contrast agent across the BBB, expressed as the transfer constant  $K_{\text{trans}}$ , can be assessed by fitting a two-compartment pharmacokinetic model to the dynamic curve of signal enhancement (4). Dynamic contrast-enhanced MRI has been successfully applied in imaging studies of brain tumor (5), in which a relatively high degree of BBB leakage is expected. However, in populations where subtle changes of BBB permeability are expected, such as aging and dementia, dynamic contrast-enhanced MRI evidence of a leaky BBB has been less convincing (6). One explanation is that the sensitivity of dynamic contrast-enhanced MRI may not be adequate to detect subtle changes in BBB permeability due to insufficient leakage of contrast agent into the interstitial space. Detecting such changes likely requires the use of small solutes with less encumbered movement across the BBB.

A potential alternative to contrast agents is water, which is able to cross the intact BBB by diffusion. However, water transport across the BBB is slower than in other vascular beds, as the tight junctions of the BBB prevent filtration by hydrostatic or osmotic pressure gradients (1). Additionally, the multiple layers of the barrier, including the endothelium and the basement membrane, all hinder water movement (7). These findings suggest that measuring the water exchange rate could be a sensitive marker of subtle changes in BBB integrity. Indeed, changes in water exchange rate were observed within 1 h of ischemia in a rat stroke model before the leakage of Gd-DTPA (8).

Arterial spin labeling (ASL) approaches have been proposed for measuring water exchange across the BBB. Although ASL is predominately considered as a perfusion technique (9), it is in principle sensitive to water exchange because of significant signal contributions from labeled water in blood and tissue (10–12). The sensitivity of the ASL signal to these two pools can be altered using diffusion weighting gradients (13). We have applied this method to study the rate of water exchange in the human brain (14). A series of ASL scans with different diffusion weightings were acquired to separate the vascular (i.e., fast diffusion) and the tissue (i.e., slow diffusion) components. The water exchange rate was determined using a tracer kinetic model to characterize the vascular signal fraction (10).

<sup>1</sup>Lawson Health Research Institute, London, Ontario, Canada.

<sup>2</sup>Ottawa Health Research Institute, Ottawa, Ontario, Canada.

<sup>3</sup>University of California Los Angeles, Los Angeles, California, USA.

Grant sponsor: Canadian Institutes of Health Research; Grant sponsor: Pilot Projects in Aging; Grant sponsor: US National Institutes of Health; Grant numbers: MH080892, AG01657011A; Grant sponsor: The America Recovery and Reinvestment Act; Grant number: MH080892-S1.

\*Correspondence to: Dr. Keith S. St. Lawrence, Lawson Health Research Institute, St. Joseph's Health Care London, 268 Grosvenor Street, London, ON N6A 4V2, Canada. E-mail: kstlaw@lawsonimaging.ca

Received 28 April 2011; revised 13 June 2011; accepted 27 June 2011.

DOI 10.1002/mrm.23104

Published online 19 August 2011 in Wiley Online Library (wileyonlinelibrary.com).

Although the results of the previous study were promising (14), the limited data that could be collected within a reasonable scanning duration resulted in some simplifications to the kinetic model that is used to characterize the DW ASL data. Specifically, it was necessary to assume that no labeled water remained in the arterial blood, and the arterial transit time was known. Both factors have been shown to significantly affect the accuracy of ASL perfusion measurements (15,16). To address these issues, we propose a two-stage method using a combination of flow-encoding gradients and postlabeling delays. In the first stage, the strength of the flow-encoding gradient was chosen to suppress spins moving in larger feeding vessels, and a relatively short postlabeling delay ensured signal from both the arterial and capillary/tissue compartments. The arterial transit time can be determined from the ratio of ASL images acquired with and without diffusion weighting (17). The second stage was similar, except the postlabeling delay was increased to allow time for the labeled water to reach the tissue compartment, and the strength of the flow-encoding gradient was increased to suppress spins moving through the microvasculature. The tracer kinetic model used to determine the water exchange rate, which is referred to as the single-pass approximation model, was modified to incorporate arterial transit times. To improve the sensitivity of the technique, DW-ASL images were acquired using pseudo-continuous ASL (pCASL) to increase labeling efficiency (18,19), background suppression to improve temporal stability (20,21), and a phased array receiver coil to achieve a higher signal-to-noise ratio (SNR) (22). This study presents the application of this two-stage approach to measuring water exchange rates in the human brain, as well as error analysis to assess the feasibility and limitations of this approach.

## THEORY

The arterial transit time ( $\tau_a$ ) was determined using the flow-encoding arterial spin tagging (FEAST) method, which is outlined in detail in Ref. 17. This section outlines the single-pass approximation model solution used to determine the water exchange rate (10). The ASL signal,  $\Delta M(t)$ , is related to the arterial concentration of labeled water through the equation

$$\Delta M(t) = CBF \int_0^t q(u) \Delta M_a(t-u) du, \quad [1]$$

where  $\Delta M_a(t)$  is the difference in arterial blood magnetization between control and label procedures and  $q(t)$  is the impulse residue function. The impulse residue function represents the concentration in the tissue volume following an idealized impulse input of unit mass and is defined in terms of capillary and brain tissue components ( $q_c(t)$  and  $q_b(t)$ , respectively) to account for the exchange of labeled water between blood and surrounding tissue:

$$\begin{aligned} q_c(t) &= e^{-\alpha t} \\ q_b(t) &= \beta [e^{-R_{1b}t} - e^{-\alpha t}] \end{aligned} \quad [2]$$

Table 1  
Definitions of parameters

$V_c$	Distribution volume of water tracer in capillary space	mL/100g
CBF	Cerebral blood flow	mL/100g/min
$PS_w$	Capillary permeability surface-area product of water	mL/100g/min
$k_w$	Exchange rate of water from blood to tissue = $PS_w/V_c$	$\text{min}^{-1}$
$\lambda$	Blood-brain partition coefficient of water	mL/100 g
$R_{1b}$	Longitudinal relaxation rate in brain tissue	$\text{s}^{-1}$
$R_{1a}$	Longitudinal relaxation rate in arterial blood	$\text{s}^{-1}$
$\delta R_1$	$R_{1a} - R_{1b}$	$\text{s}^{-1}$
$\delta$	Duration of the arterial spin labeling	s
$\tau_a$	Transit time to the capillary-tissue compartment	s
$\alpha$	Model parameter = $k_w + R_{1a}$	$\text{s}^{-1}$
$\beta$	Model parameter = $\frac{k_w}{k_w + \delta R_1}$	

where  $R_{1b}$  is the longitudinal relaxation rate of brain tissue and the parameters  $\alpha$  and  $\beta$  are defined in Table 1. Both  $\alpha$  and  $\beta$  depend on the rate of water exchange from blood to tissue, defined as  $k_w$  in Table 1. In turn,  $k_w$  equals the permeability-surface area product of water ( $PS_w$ ) divided by the capillary blood volume ( $V_c$ ) (10). To simplify the solution to Eq. 1, these equations are based on the assumption that the vascular transit time is longer than the acquisition time, which is reasonable considering that venous outflow is negligible at typical flow rates in the human brain (23). Figure 1 shows an example of  $q_c(t)$  and  $q_b(t)$  as predicted by Eq. 2. Because labeled water enters the tissue volume via the blood supply,  $q_c(t) = 1$  and  $q_b(t) = 0$  at time zero. As the labeled water flows through the capillary space,  $q_c(t)$  continually decreases due to the diffusion of labeled water into the surrounding tissue and T1 relaxation of blood. At the same time,  $q_b(t)$  increases due to the influx of labeled water; however, this increase is counteracted by T1 relaxation of tissue.

For pseudo-continuous ASL (pCASL),  $\Delta M_a(t)$  is defined as

$$\Delta M_a(t) = \begin{cases} 0 & 0 < t < \tau_a \\ -\frac{2\varepsilon M_0}{\lambda} e^{-R_{1a}\tau_a} & \tau_a \leq t \leq \delta + \tau_a \\ 0 & \delta + \tau_a < t \end{cases} \quad [3]$$

where  $\varepsilon$  is the tagging efficiency (19),  $M_0$  is the tissue equilibrium magnetization,  $\lambda$  is the partition coefficient of water in brain,  $R_{1a}$  is the longitudinal relaxation rate of arterial blood, and  $\delta$  is the duration of the labeling period. In this study, the postlabeling delay ( $\tau_d$ ) was long enough to allow all of the labeled water time to reach the tissue (i.e.,  $t > \delta + \tau_a$ ). Under this condition, the ASL contributions from the capillary space,  $\Delta M_c(t)$ , and the tissue space,  $\Delta M_b(t)$ , are given by

$$\Delta M_c(t) = -\frac{2CBF\varepsilon M_0}{\lambda\alpha} e^{-(R_{1a}-\alpha)\tau_a} (e^{-\alpha(t-\delta)} - e^{-\alpha t}), \quad [4]$$

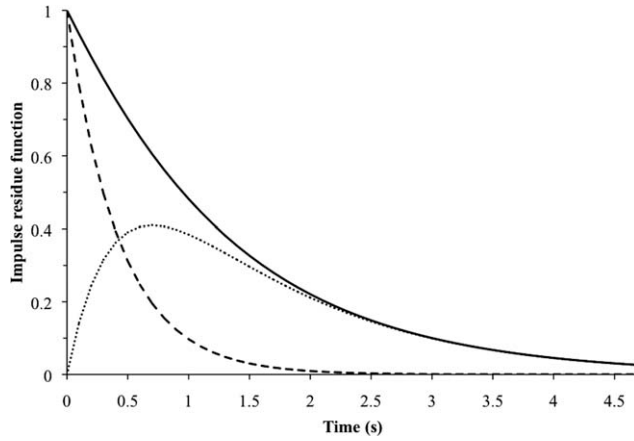


FIG. 1. Illustrated example of the impulse residue function ( $q(t)$ , solid line) and its capillary ( $q_c(t)$ , dashed line) and tissue ( $q_t(t)$ , dotted line) components as defined by Eq. (2). In this example, CBF = 50 mL/100g/min, PS = 150 mL/100g/min,  $V_c = 2.0$  mL/100g,  $T_{1a} = 1.5$  s, and  $T_{1b} = 1.26$  s.

$$\Delta M_b(t) = -\frac{2CBF\varepsilon M_0\beta}{\lambda} \left[ \frac{e^{-(R_{1a}-R_{1b})\tau_a}}{R_{1b}} \left( e^{-R_{1b}(t-\delta)} - e^{-R_{1b}t} \right) - \frac{e^{-(R_{1a}-\alpha)\tau_a}}{\alpha} \left( e^{-\alpha(t-\delta)} - e^{-\alpha t} \right) \right]. \quad (5)$$

With DW-ASL, it is assumed that  $\Delta M_c(t)$  and  $\Delta M_b(t)$  can be separated by their different sensitivities to flow-encoding gradients. Consequently, the ASL signal collected at a given postlabeling delay and with multiple diffusion-weightings (i.e.,  $b$  values) can be characterized by a bi-exponential model (14):

$$\frac{\Delta M(t, b)}{\Delta M(t, 0)} = A_1(t)e^{-bD_1} + A_2(t)e^{-bD_2}, \quad (6)$$

where the weighting factors  $A_1$  and  $A_2$  are the fractions of the fast (vascular) and slow (tissue) components of the signal attenuation curve, respectively ( $A_1 + A_2 = 1$ ), and  $D_1$  and  $D_2$  are the corresponding apparent diffusion coefficients. Using the definitions of  $\Delta M_c(t)$  and  $\Delta M_b(t)$  provided in Eqs. 4 and 5, the weighting factors are given by

$$A_1(t) = \frac{\Delta M_c(t)}{\Delta M_c(t) + \Delta M_b(t)} \quad \text{and} \quad A_2(t) = \frac{\Delta M_b(t)}{\Delta M_c(t) + \Delta M_b(t)}. \quad (7)$$

These terms are functions of time since their relative magnitude will change with the duration of the postlabeling delay. That is,  $A_1$  will decrease with longer postlabeling delays as the labeled water diffuses from the microvasculature into the tissue. The weighting factors can be determined by fitting Eq. (6) to  $\Delta M$  data acquired at multiple  $b$  values ranging from 0 to 300 s/mm<sup>2</sup> (14). However, this is a relatively slow process and the SNR of the  $\Delta M$  data decreases with larger diffusion weighting due to the increased sensitivity to motion. An alternative procedure is to acquire  $\Delta M$  data at only two  $b$  values: zero and a larger value ( $b_{DW}$ ) sufficient to suppress the

vascular signal, but with minimum effect on the tissue signal. In this case,  $A_1$  and  $A_2$  are given by

$$A_1(t) = 1 - \frac{\Delta M(b_{DW})}{\Delta M(b_0)} \quad \text{and} \quad A_2(t) = \frac{\Delta M(b_{DW})}{\Delta M(b_0)} \quad (8)$$

The expressions for  $A_1$  and  $A_2$  contain two unknown variables:  $k_w$ , which is incorporated into the parameters  $\alpha$  and  $\beta$ , and the arterial transit time  $\tau_a$ . Figure 2 shows the dependency of the capillary fraction ( $A_1$ ) on  $k_w$  over a range from 0 to 200 min<sup>-1</sup>.

## MATERIALS AND METHODS

### Diffusion-Weighted Arterial Spin Labeling Sequence

Similar to the original study (14), the DW-ASL sequence used a combination of a continuous arterial spin labeling sequence and a twice refocused, spin-echo diffusion sequence (Fig. 3) (24). For this study, a ‘‘balanced’’ pCASL sequence was implemented consisting of 1600 selective radiofrequency pulses (Hanning-shaped pulses with duration of 500  $\mu$ s, spacing of 920  $\mu$ s, peak  $B_1$  of 5.3  $\mu$ T, and average  $B_1$  of 1.8  $\mu$ T) (19,25). The train of radiofrequency pulses was performed in conjunction with a slice-selective gradient (6.0 mT/m) for a total duration of 1.5 s. The labeling plane was positioned 8 cm from the center of the imaging volume. Background suppression was achieved by applying two nonselective inversion pulses during the postlabeling delay. Hyperbolic secant pulses (duration of 15.35 ms) were implemented and the timings of the background suppression pulses for each postlabeling delay were chosen to suppress grey and white matter signals in the first imaging slice (26).

Interleaved images with and without labeling were acquired using a single-shot, spin-echo, echo-planar imaging (EPI) sequence with two refocusing pulses. Two pairs of bipolar gradients were applied along the slice direction (between the excitation pulse and EPI acquisition), with the radiofrequency refocusing pulses dividing each bipolar pair. The durations of the four lobes of the bipolar gradients were optimized to minimize effects of eddy currents during EPI readout.

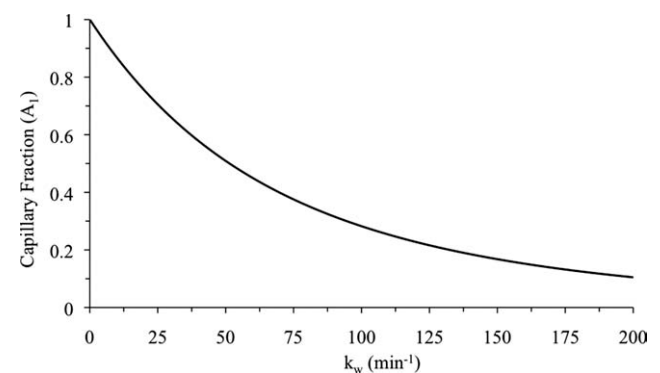


FIG. 2. Predicted capillary fraction of labeled water ( $A_1$ ) plotted as a function of the water-exchange rate ( $k_w$ ). Simulated data were generated using  $T_{1b} = 1.26$  s,  $T_{1c} = 1.5$  s, a labeling duration of 1.5 s,  $\tau_a = 1.26$  s and a postlabeling delay of 1.5 s.

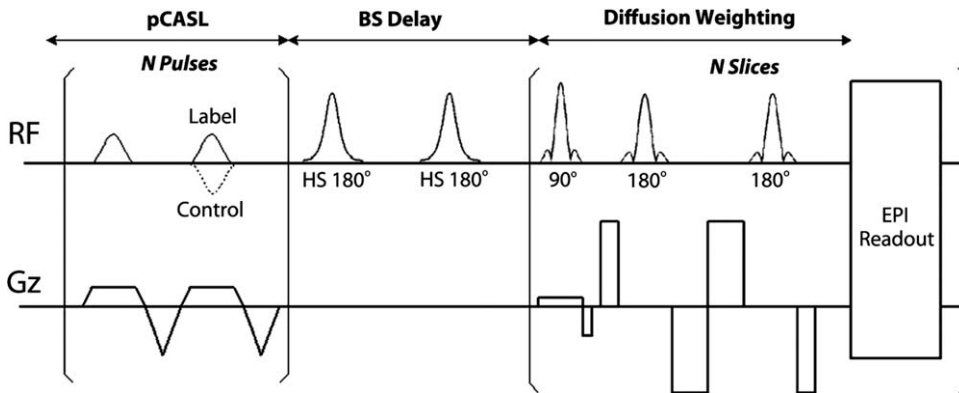


FIG. 3. DW-ASL sequence incorporated pseudo-continuous ASL (pCASL), background suppression, and twice-refocused spin-echo diffusion weighting.

### Imaging Protocols

Written informed consent was obtained before all studies according to a protocol approved by the Institutional Review Board. Each session began with the acquisition of anatomical images using a 3D MPRAGE sequence (recovery time (TR)/echo time (TE) = 2000/2.96 ms with an isotropic resolution of 1 mm).

### Multiple $b$ -Value Protocol

Diffusion-weighted pCASL data were acquired with four  $\tau_d$  values (900, 1200, 1500, and 1800 ms) and seven  $b$  values (0, 5, 10, 25, 50, 100, and 200  $\text{s/mm}^2$ ) to determine the appropriate  $b$  value for the two-stage protocol that would suppress the vascular signal contribution while having minimal effect on the tissue signal. Experiments were conducted on a Siemens 3 T Trio whole-body scanner (Siemens AG, Erlangen, Germany) employing a product eight-channel head array coil. Four healthy volunteers (average age  $26.4 \pm 3.4$  yr, two females) participated in the experiment.

The image acquisition parameters for the DW-ASL sequence were a field of view = 22 cm, a matrix =  $64 \times 64$ , bandwidth = 3kHz/pixel, 6/8 partial k-space, rate-2 GRAPPA, slice thickness = 8 mm, interslice gap = 2 mm, TE = 55 ms, and TR = 4 s. Eight slices were acquired in ascending order. Diffusion gradients were applied along the Z-axis. Control and labeled images were acquired in an alternating pattern. Eighty acquisitions were obtained for each  $\tau_d$  value combined with seven  $b$  values. The acquisition duration for each combination was 5.5 min.

### Two-Stage Protocol

Experiments were conducted on a Siemens 3 T Verio whole-body scanner (Siemens AG, Erlangen, Germany) employing a product 32-channel head array coil. Seven healthy volunteers (mean age  $28 \pm 5$  yr, three females) participated in the experiment.

The DW-pCASL images were acquired with a field of view = 24 cm, a matrix =  $64 \times 64$ , bandwidth = 3 kHz/pixel, 7/8 partial k-space, rate-2 GRAPPA, slice thickness = 8 mm, interslice gap = 2 mm, and TE = 48 ms. Eight slices were acquired in ascending order. Three sets of DW-pCASL data were collected, each with two  $b$  values. The FEAST data were acquired using  $b = 0$  and 10  $\text{s/mm}^2$  and

$\tau_d = 800$  ms, which were sufficient to allow the labeled water to reach the arterial compartment. The total acquisition time for the FEAST was 7.5 min with a TR = 3.5 s. For the second and third data sets,  $b = 0$  and 50  $\text{s/mm}^2$ —the latter value will suppress all flowing spins—and  $\tau_d = 1500$  ms to ensure all labeled water reached the tissue compartment (i.e., capillaries and surrounding tissue). For each of these sets, which are denoted DW-pCASL ( $k_w$ ), the acquisition time was 8.5 min with a TR = 4 s. Diffusion gradients were applied along the Z-axis. The flow encoding velocities for the  $b$  value of 10 and 50  $\text{s/mm}^2$  were 7 and 2 mm/s, respectively. These values were chosen to suppress spins in vessels larger than arterioles and in capillaries, respectively (27).

### Data Analysis

Raw EPI images were motion corrected and spatially filtered using SPM software (Statistical Parametric Mapping, London, UK). Images acquired under the multi  $b$ -value protocol were filtered with a 2-mm FWHM isotropic gaussian kernel, while an 8-mm smoothing kernel was used for the FEAST images acquired under the two-stage protocol (i.e.,  $b = 0$  and 10  $\text{s/mm}^2$ ). The kernel size was increased to 15 mm used for the DW-ASL ( $k_w$ ) images (i.e.,  $b = 0$  and 50  $\text{s/mm}^2$ ) to improve the precision of the  $k_w$  estimates (see error analysis section). Processed EPI images were pair-wise subtracted and time averaged to generate mean ASL images ( $\Delta M$ ) for each  $b$  value.

The SPM software was used to segment the anatomical images into regions of interests (ROIs) representing grey matter, white matter, and cerebrospinal fluid. The ROIs were applied to the multi  $b$ -value  $\Delta M$  images to extract mean  $\Delta M$  values in grey and white matter for each of the seven  $b$  values. Equation 6 was fit to the  $\Delta M$  series to extract estimates of the weighting factors ( $A_1$  and  $A_2$ ) and the apparent diffusion coefficients ( $D_1$  and  $D_2$ ). The fitting procedure was performed using software written in IDL (Interactive Data Language, Research Systems, Boulder, CO) and conducted on each subject's data, as well as the  $\Delta M$  signal averaged across all subjects.

ROI analysis was also conducted on the images acquired under the two-stage protocol to obtain mean values of  $\tau_a$  and  $k_w$  for grey and white matter. Arterial transit time was determined from the FEAST images (17). This analysis accounted for the delay of 87 ms

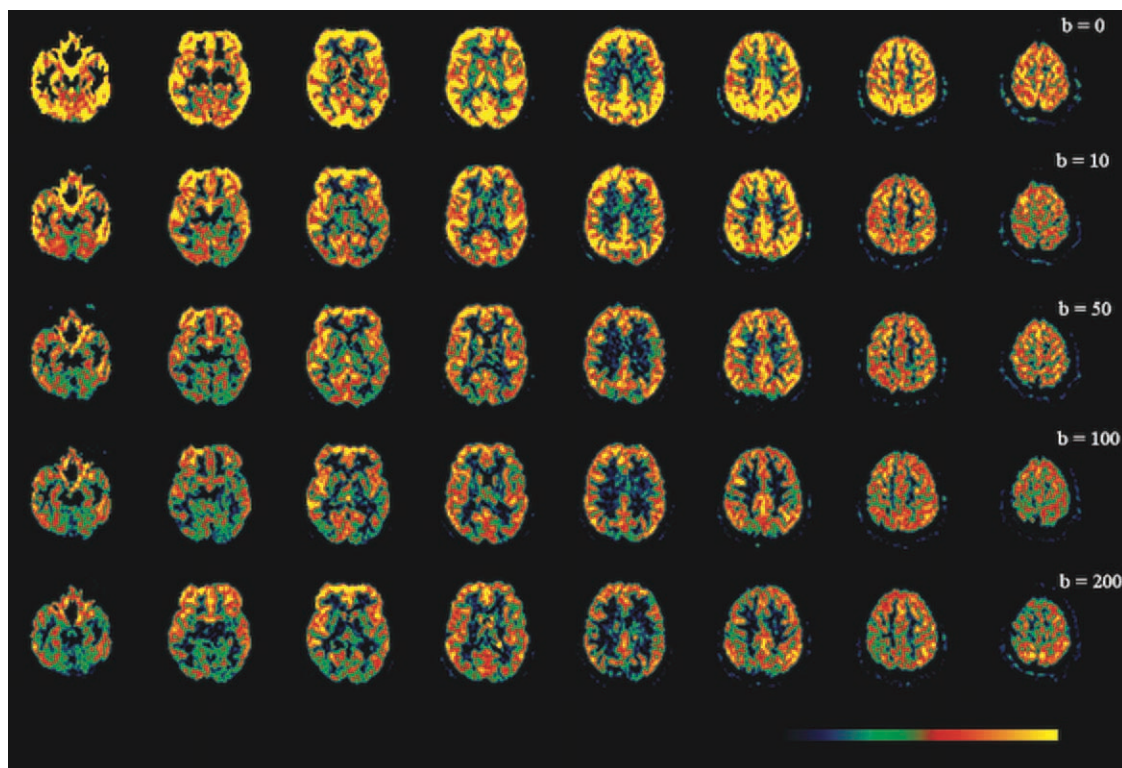


FIG. 4. Average  $\Delta M$  images acquired under the multiple  $b$  value protocol from one individual with the delay of 1200 ms. Images from five  $b$  values are presented to illustrate the general effect of varying the diffusion weighting. [Color figure can be viewed in the online issue, which is available at [wileyonlinelibrary.com](http://wileyonlinelibrary.com).]

between the acquisition of successive slices. Grey and white matter  $k_w$  values were determined by comparing the measured capillary fraction,  $A_1$ , to a table of  $A_1$  values generated from Eq. 8 using the measured  $\tau_a$  and a range of  $k_w$  values (0.01 to 500  $\text{min}^{-1}$ ). The upper limit was deemed sufficient to characterize complete extraction of labeled water into the tissue during a single capillary transit (28). The  $A_1$  values were generated assuming  $T_1$  values of grey matter, white matter, and blood equal to 1.26, 0.85, and 1.49 s, respectively (29,30). Mean  $k_w$  values were determined separately for the two sets of DW-ASL ( $k_w$ ) data to assess reproducibility. Using the same look-up table approach, images of  $\tau_a$  and  $k_w$  were generated from the FEAST and DW-ASL ( $k_w$ ) images, respectively. For the latter, the two data sets were combined to improve the SNR and the average  $\tau_a$  in each slice was used to generate the corresponding  $k_w$  image.

#### Error Analysis

Monte Carlo simulations were conducted to assess the accuracy and the precision of the  $k_w$  measurements. A set of 5000  $A_1$  values was generated from Eqs. 4, 5, and 8 assuming  $k_w = 100 \text{ min}^{-1}$ ,  $\tau_a = 1.2 \text{ s}$ ,  $\tau_d = 1.5 \text{ s}$ ,  $\delta = 1.5 \text{ s}$ , grey matter  $T_1 = 1.26 \text{ s}$ , and blood  $T_1 = 1.49 \text{ s}$ . Random gaussian noise was added to the  $A_1$  values, and  $k_w$  estimates were determined from the noisy data using the same look-up table approach used to analyze the experimental data. Simulations were conducted over a range of noise levels. For comparison, the standard deviation of the filtered  $\Delta M$  images,  $\sigma(\Delta M)$ , was measured in the FEAST

and DW-ASL( $k_w$ ) time series. The analysis was conducted across all pixels in grey and white matter ROIs.

#### RESULTS

Figure 4 shows average  $\Delta M$  images from one subject under the multiple  $b$  value protocol to illustrate the signal reduction as the strength of the diffusion-weighting gradient increased. Bi-exponential fitting was successfully applied to the grey and white matter  $\Delta M$  data from each subject. Figure 5 shows the average  $\Delta M$  series acquired at four  $\tau_d$  values. The magnitude of the fast component (i.e., the vascular contribution) diminished with longer postlabeling delays due to increased extraction of labeled water into the tissue. The best-fit estimates of the fast ( $D_1$ ) and slow ( $D_2$ ) apparent diffusion coefficients from these data sets are provided in Table 2, along with the corresponding vascular fraction  $A_1$ . The  $D_1$  value varied considerably between the different  $\Delta M$  series, likely reflecting the difficulty of characterizing this fast component; however,  $D_1$  was always much greater than  $D_2$ . For example, the  $D_1$  and  $D_2$  values at  $\tau_d = 1500 \text{ ms}$ , which was the postlabeling delay used with the two-stage protocol, indicated that a  $b$  value of 50  $\text{s/mm}^2$  would be sufficient to separate the vascular and tissue signal contributions. At this  $b$  value, the average vascular and tissue contributions in grey matter were less than 0.2% and greater than 94%, respectively.

Individual  $\tau_a$  and  $k_w$  measurements in grey and white matter from all subjects are presented in Table 3. These measurements were obtained by ROI analysis of the

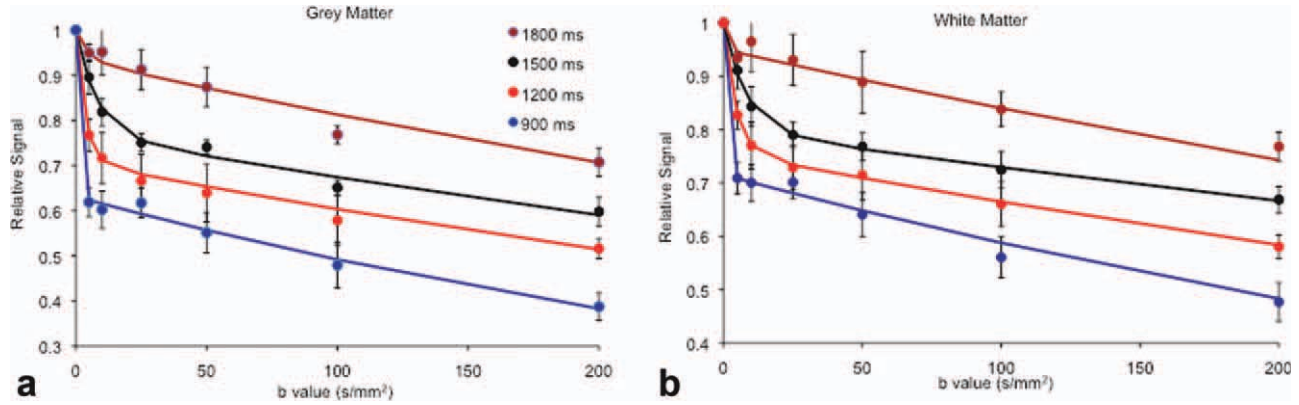


FIG. 5. Average  $\Delta M$  signal (symbols) acquired at four postlabeling delays plotted as a function of diffusion-weighting strength. Data were averaged across all pixels in grey matter, **a**, or white matter, **b**, and across four subjects. Each subject's data were normalized to the signal without diffusion weighting ( $b = 0$ ). The errors bars represent the standard error. The solid lines represent the best fit of a bi-exponential decay model (Eq. 6) to each  $\Delta M$  series. [Color figure can be viewed in the online issue, which is available at [wileyonlinelibrary.com](http://wileyonlinelibrary.com).]

$\Delta M(b_{10})/\Delta M(b_0)$  and  $\Delta M(b_{50})/\Delta M(b_0)$  images, respectively. Using a two-tailed paired  $t$  test, no significant differences were found between grey and white matter  $\tau_a$  measurements or between grey and white matter  $k_w$  measurements. Average  $\Delta M(b_{10})/\Delta M(b_0)$  and  $\Delta M(b_{50})/\Delta M(b_0)$  values across the whole brain were  $0.58 \pm 0.05$  and  $0.72 \pm 0.08$ , respectively. The intrasubject coefficient of variation determined from the two DW-ASL ( $k_w$ ) data sets was  $26\% \pm 23\%$  in grey matter and  $21\% \pm 17\%$  in white matter.

Representative FEAST and DW-ASL( $k_w$ ) images from one subject are shown in Fig. 6a and b, respectively. Each set of images includes the diffusion-weighted images ( $\Delta M(b_0)$  and  $\Delta M(b_{DW})$ ), the  $\Delta M(b_{DW})/\Delta M(b_0)$  images, and either (a) the  $\tau_a$  images or (b) the  $k_w$  images. In this example, whole brain  $\Delta M(b_{10})/\Delta M(b_0) = 0.57$  and  $\Delta M(b_{50})/\Delta M(b_0) = 0.74$ . Average grey and white matter values from the  $k_w$  images for all subjects are presented in Table 4. Similarly to the previous ROI analysis, there was no statistically significant difference between the grey and white matter  $k_w$  values. However, these values were significantly higher than the corresponding values derived from the  $\Delta M(b_{50})/\Delta M(b_0)$  images (Table 3). This bias was caused by pixels with  $k_w$  values that reached the upper limit of  $500 \text{ min}^{-1}$ . In those pixels, the  $\Delta M(b_{50})/\Delta M(b_0)$  ratio was close to or greater than 1, likely due to noise contributions. Example histograms of the  $\Delta M(b_{50})/\Delta M(b_0)$  ratio and the corresponding  $k_w$

values from subject 7 are shown in Fig. 7. Approximately 5% of the  $\Delta M(b_{50})/\Delta M(b_0)$  values were greater than 1 in this case, which is the same fraction of  $k_w$  values equal to  $500 \text{ min}^{-1}$ .

Mean pixel SNR measurements from the four acquired  $\Delta M$  sets are given in Table 5. As expected, the FEAST  $\Delta M$  images have higher SNRs than the corresponding DW-ASL( $k_w$ ) images due to the shorter post-labeling delay and smaller  $b$  value used with the former. Because of the higher SNR, no significant differences were found between grey and white matter values from the  $\tau_a$  images ( $1.49 \pm 0.08$  and  $1.48 \pm 0.04$  s, respectively) and those values derived from the  $\Delta M(b_{10})/\Delta M(b_0)$  images (Table 3).

Results of the Monte Carlo simulations used to assess the accuracy and precision of the  $k_w$  measurements are shown in Fig. 8. The range of  $k_w$  estimates are plotted as a function of the coefficient of variation of  $A_1$ . As coefficient of variation increased, the number of  $A_1$  values close to or greater than 1 increased, resulting in a skewed distribution of  $k_w$  estimates with a cluster of values at the upper limit ( $500 \text{ min}^{-1}$ ) and a bias in the mean value. For comparison, the mean coefficient of variation of  $A_1$  derived from the SNR calculations given in Table 5 was  $0.62 \pm 0.10$ . Figure 8 predicts a bias of

Table 2  
Parameters characterizing the  $\Delta M$  decay in grey and white matter regions of interest

	Grey matter			White matter		
	$D_1$ ( $\text{mm}^2/\text{s}$ )	$D_2$ ( $\text{mm}^2/\text{s}$ )	$A_1$	$D_1$ ( $\text{mm}^2/\text{s}$ )	$D_2$ ( $\text{mm}^2/\text{s}$ )	$A_1$
$\tau_d$ (ms)						
900	493	0.0025	0.37	1.1	0.00196	0.29
1200	0.3	0.0016	0.29	0.235	0.0013	0.24
1500	0.125	0.0013	0.23	0.123	0.0009	0.20
1800	0.23	0.0014	0.06	54.51	0.00123	0.05

Values were obtained from the analysis of the  $\Delta M$  signal averaged across four subjects.

Table 3  
Average transit time ( $\tau_a$ ) and water exchange rate ( $k_w$ ) in grey and white matter regions of interest

Subject	$\tau_a$ (s)		$k_w$ ( $\text{min}^{-1}$ )	
	Grey matter	White matter	Grey matter	White matter
1	1.57	1.65	81	110
2	1.56	1.53	116	123
3	1.41	1.45	127	146
4	1.50	1.43	100	125
5	1.52	1.54	108	135
6	1.50	1.57	121	98
7	1.36	1.52	124	144
Mean	$1.49 \pm 0.08$	$1.53 \pm 0.07$	$110 \pm 18$	$126 \pm 18$

The  $\tau_a$  and  $k_w$  values were obtained from the ROI analysis of the  $\Delta M(b_{10})/\Delta M(b_0)$  and  $\Delta M(b_{50})/\Delta M(b_0)$  images, respectively.

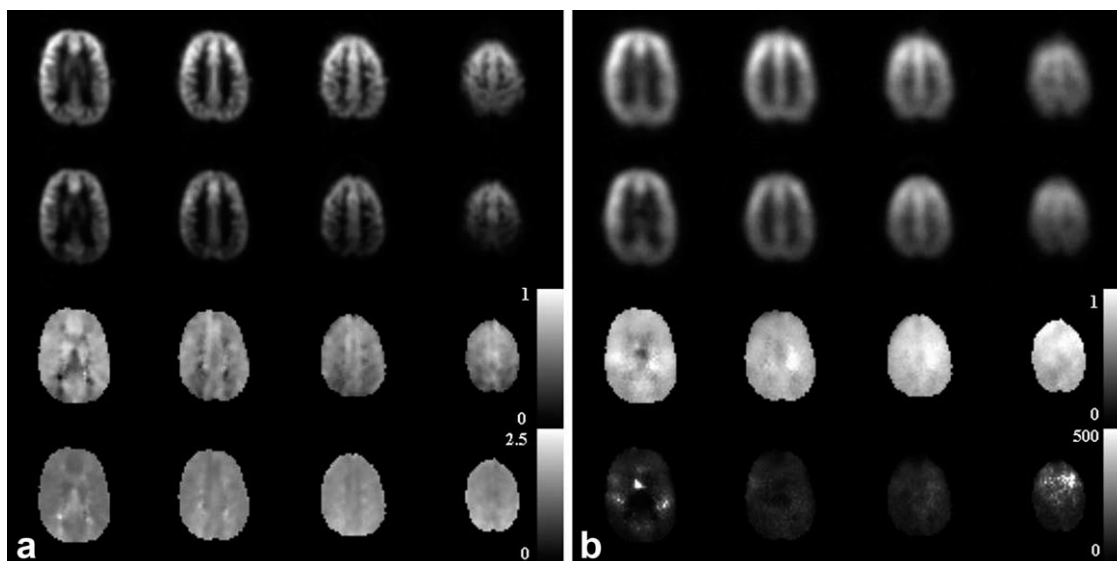


FIG. 6. DW-ASL  $\Delta M$  images from one subject: **a**: FEAST data acquired with  $\tau_d = 0.8$  s and **b**: DW-ASL ( $k_w$ ) data acquired with  $\tau_d = 1.5$  s. Each set shows the average diffusion-weighted  $\Delta M$  images,  $\Delta M(b_0)$  in the first row and  $\Delta M(b_{DW})$  in the second row; the ratio images  $\Delta M(b_{DW})/\Delta M(b_0)$  are in the third row; and either the (a)  $\tau_a$  or (b)  $k_w$  images are in the final row (the  $\tau_a$  scale is in units of seconds and the  $k_w$  scale in  $\text{min}^{-1}$ ). Four of eight slices are shown. All images were smoothed with a gaussian filter with a kernel size of 8 mm for the FEAST images and 15 mm for the DW-ASL( $k_w$ ) images. Images were generated using  $T_1$  values of 1.26, 0.85, and 1.49 s for grey matter, white matter, and blood, respectively.

approximately 36% at this coefficient of variation value with approximately 5% of the  $k_w$  estimates at the upper level. Both of these predictions are similar to the experimental results presented in Table 4 and Fig. 7.

### DISCUSSION

Analogous to ASL blood flow measurements, the accuracy of DW-ASL  $k_w$  measurements can be affected by the arterial transit time and signal contributions from arterial blood. We have attempted to minimize these confounding effects by directly measuring  $\tau_a$  and by choosing a postlabeling delay greater than  $\tau_a$ . The latter ensures that all labeled water reaches the capillary space, where it can diffuse across the blood-brain barrier into tissue. The signal equations that characterize the amount of labeled water in these two spaces were modified to account for both of these timing variables (Eqs. 4 and 5). In this study, the chosen postlabeling delay ( $\tau_d = 1.5$  s) was sufficient to satisfy the second criterion for all subjects—

note, some of the  $\tau_a$  values given in Table 3 are greater than 1.5 s because these values were averaged across all slices. If the duration of the postlabeling delay had not been sufficient, an alternative approach would be to use a serial compartment model as originally proposed for cerebral blood flow measurements (16). In the case of DW-ASL, the first compartment would represent the arterial contribution and the second compartment would represent the capillary/tissue contributions.

The average values of  $\tau_a$  in grey and white matter obtained with the FEAST technique (Table 3) were in good agreement with our previous results (17), which were also obtained using continuous ASL with a labeling distance of 8 cm. It was anticipated that  $\tau_a$  would be greater in white matter than grey matter. The lack of a difference between the two tissues was likely due to the poorer SNR in white matter voxels and signal contamination from grey matter caused by spatial filtering. Partial volume errors can also result from signal contamination from cerebrospinal fluid. However, this error is caused primarily by incorrectly estimating  $M_0$  and, therefore, it should have minimal effect on  $\tau_a$  and  $k_w$  (31). In contrast to the  $\tau_a$  measurements, our previous estimation of grey matter  $k_w$  ( $193 \pm 50 \text{ min}^{-1}$ ) is larger than the average value obtained by ROI analysis in the present study (14). In the previous study,  $k_w$  was determined using an assumed arterial transit time ( $\tau_a = 1.4$  s), a shorter post-labeling delay ( $\tau_d = 1.2$  s), and a version of the single-pass approximation model that did not account for signal contributions from labeled water in arterial blood when  $\tau_d < \tau_a$ . Explicitly accounting for these factors in this study likely resulted in more accurate measurements.

An estimation of the permeability-surface area product of water can be derived from  $k_w$  by assuming a known value for the microvasculature blood volume. Reported

Table 4  
Average grey and white matter values determined from the  $k_w$  images

Subject	$k_w$ ( $\text{min}^{-1}$ )	
	Grey matter	White matter
1	94	119
2	147	203
3	156	156
4	112	119
5	155	224
6	158	104
7	151	157
Mean	$139 \pm 25$	$154 \pm 45$

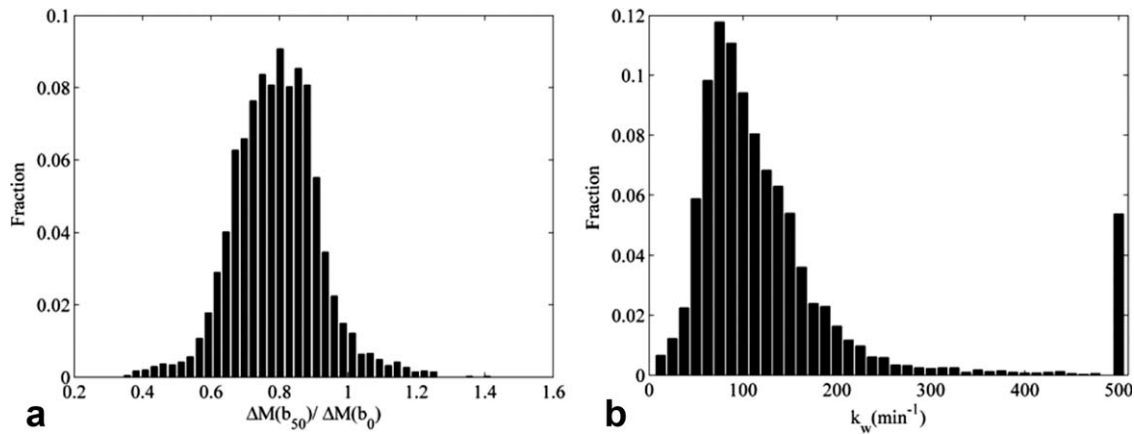


FIG. 7. **a**: Histogram of  $\Delta M(b_{50})/\Delta M(b_0)$  values across all pixels from one subject's data. The ordinate represents the relative number of pixels at a given  $\Delta M(b_{50})/\Delta M(b_0)$  value. **b**: Histogram of corresponding  $k_w$  values.

values of  $V_c$  in the cerebral cortex of cats are typically 1.5 to 2 mL/100 g (27). Using this range and the mean grey matter  $k_w$  value given in Table 3,  $PS_w$  would be between 165 to 220 mL/100 g/min, which is in reasonable agreement with previously reported values: 127 mL/100 g/min in humans (32), 138 mL/100 g/min in monkeys (33), 140 mL/100 g/min in rabbits (34), and between 138 to 319 mL/100 g/min in rats (35,36). Assuming a grey-to-white matter blood volume ratio of 2:1 (37), the estimated  $PS_w$  in white matter would be between 95 to 126 mL/100 g/min, which is similar to the value of 80 mL/100g/min reported by Herscovitch et al. (32). The general agreement between our results and previous measurements of  $PS_w$  suggests that DW-ASL can accurately measure the water exchange rate. The next step will be to determine if the technique is sensitive to changes in BBB permeability, such as caused by infusing hypertonic mannitol, or if  $k_w$  is linearly correlated with regional variations in CBF as previously reported for  $PS_w$  (32).

The primary challenge to measuring  $k_w$  by ASL is achieving an acceptable degree of precision due to the inherently poor SNR of ASL. The first ASL study to measure  $k_w$  acquired data at multiple postlabeling delays and included  $PS_w$  as an additional fitting parameter (23). Large intersubject variability was found with this approach and it has been suggested that it lacks the sensitivity to measure  $PS_w$  with reasonable precision (38). The poor sensitivity can, in part, be attributed to the relatively small differences in blood and tissue relaxation times, which makes it difficult to distinguish the two pools. The use of diffusion weighting gradients enhances this signal differences. In this study, the average decrease in the  $\Delta M$  signal caused by applying DW gra-

dients with  $b = 50$  s/mm<sup>2</sup> was 28%. However, this approach is also SNR limited because the estimation of  $k_w$  is based on the ratio of two  $\Delta M$  images, one of which has lower a SNR due to diffusion weighting (Table 5). This SNR limitation manifested as a bias in the mean value of the  $k_w$  images and a large coefficient of variation. For example, the five and nine percentiles from the data presented in Fig. 7 were 52 and 500 min<sup>-1</sup>, respectively. The latter percentile had reached the upper limit set in the fitting algorithm and pixels at the upper limit are evident in the  $k_w$  images by bright artifacts (Fig. 6). Similar effects due to image noise were predicted by the Monte Carlo simulations. The simulations also demonstrated that minimizing the bias and reducing the 5 and 95 percentiles to less than  $\pm 25\%$  would require reducing the coefficient of variation to below 0.2. This reduction can be achieved by ROI analysis, such as the grey and white matter results presented in Table 3. In this study, separate ROI analysis of the two DW-ASL( $k_w$ ) data sets indicated a test-retest coefficient of variation of 26% in grey matter and 25% in white matter. These results demonstrate that DW-ASL can produce reproducible  $k_w$  values, at least in large regions of interest. Achieving

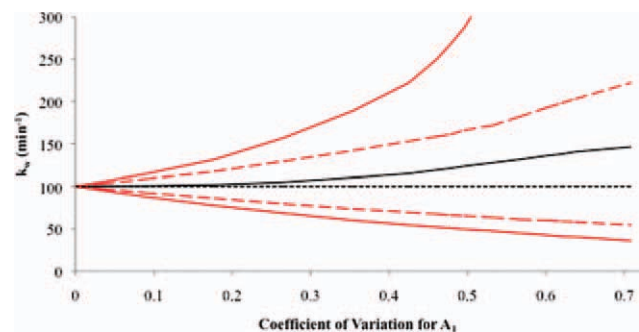


FIG. 8. Error in water-exchange rate  $k_w$  due to random noise added to the capillary fraction ( $A_1$ ) signal. The dotted black line represents the input  $k_w$  value and the solid black line represents the mean value from the simulations. The two dashed red lines are the 16 and 84 percentiles and the two solid red lines are the 5 and 95 percentiles. [Color figure can be viewed in the online issue, which is available at [wileyonlinelibrary.com](http://wileyonlinelibrary.com).]

Table 5  
Mean pixel SNR in each DW-ASL image set

Image series	SNR
FEAST $\Delta M(b_0)$	$3.08 \pm 0.70$
FEAST $\Delta M(b_{10})$	$1.53 \pm 0.34$
DW-ASL( $k_w$ ) $\Delta M(b_0)$	$1.96 \pm 0.39$
DW-ASL( $k_w$ ) $\Delta M(b_{50})$	$0.84 \pm 0.18$

Values were averaged across seven subjects.

comparable levels of precision at a pixel-by-pixel level will clearly require greater sensitivity. One immediate improvement would be to incorporate DW-ASL with single-shot 3D imaging, which has been shown to significantly improve temporal SNR (39). Another alternative for future clinical applications would be to use  $\Delta M(b_{50})/\Delta M(b_0)$  as a surrogate marker of water exchange since the  $\Delta M(b_{50})/\Delta M(b_0)$  images demonstrated superior spatial homogeneity compared with the  $k_w$  maps (see Fig. 6b). In previous animal studies, the ratio of the tissue-compartment ASL signal to the total ASL signal has been used to estimate the water extraction fraction (E) based on the assumption of instantaneous extraction across the BBB (13,40).

One limitation of this study was that the diffusion gradients were applied along the z-axis, with the assumption that microvascular flow is isotropic. In future studies, diffusion gradients can be applied along two or three directions, which would simultaneously shorten the echo time. Nevertheless, our recent multidirectional DW-pCASL data acquired with six non-collinear directions suggested no evidence of anisotropic microvascular flow (41).

In summary, this study investigated the feasibility of a two-stage DW-ASL procedure for measuring both  $\tau_a$  and  $k_w$ . The  $\tau_a$  estimates were in good agreement with our previous results (17), and the  $k_w$  values compared favorably with  $PS_w$  measurements from positron emission tomography (32). The reproducibility of regional  $k_w$  values was reasonable, as determined from the intrasubject coefficients of variation; however, SNR analysis and Monte Carlo simulations indicated that the sensitivity of the technique needs to be improved to provide pixel  $k_w$  values with acceptable precision.

## ACKNOWLEDGMENTS

The authors thank J. Miller for her help with data collection.

## REFERENCES

- Paulson OB. Blood-brain barrier, brain metabolism and cerebral blood flow. *Eur Neuropsychopharmacol* 2002;12(6):495–501.
- Weiss N, Miller F, Cazaubon S, Couraud PO. The blood-brain barrier in brain homeostasis and neurological diseases. *Biochim Biophys Acta* 2009;1788(4):842–857.
- Rebeles F, Fink J, Anzai Y, Maravilla KR. Blood-brain barrier imaging and therapeutic potentials. *Top Magn Reson Imaging* 2006;17(2):107–116.
- Tofts PS, Kermode AG. Measurement of the blood-brain barrier permeability and leakage space using dynamic MR imaging. 1. Fundamental concepts. *Magn Reson Med* 1991;17(2):357–367.
- Barrett T, Brechbiel M, Bernardo M, Choyke PL. MRI of tumor angiogenesis. *J Magn Reson Imaging* 2007;26(2):235–249.
- Starr JM, Farrall AJ, Armitage P, McGurn B, Wardlaw J. Blood-brain barrier permeability in Alzheimer's disease: a case-control MRI study. *Psychiatry Res* 2009;171(3):232–241.
- Li G, Yuan W, Fu BM. A model for the blood-brain barrier permeability to water and small solutes. *J Biomech* 2010;43(11):2133–2140.
- Kim YR, Tejima E, Huang S, Atochin DN, Dai G, Lo EH, Huang PL, Bogdanov A, Jr., Rosen BR. In vivo quantification of transvascular water exchange during the acute phase of permanent stroke. *Magn Reson Med* 2008;60(4):813–821.
- Barbier EL, Lamalle L, Decors M. Methodology of brain perfusion imaging. *J Magn Reson Imaging* 2001;13(4):496.
- St Lawrence KS, Frank JA, McLaughlin AC. Effect of restricted water exchange on cerebral blood flow values calculated with arterial spin tagging: a theoretical investigation. *Magn Reson Med* 2000;44(3):440–449.
- Ewing JR, Cao Y, Fenstermacher J. Single-coil arterial spin-tagging for estimating cerebral blood flow as viewed from the capillary: relative contributions of intra- and extravascular signal. *Magn Reson Med* 2001;46(3):465.
- St Lawrence KS, Wang J. Effects of the apparent transverse relaxation time on cerebral blood flow measurements obtained by arterial spin labeling. *Magn Reson Med* 2005;53(2):425–433.
- Silva AC, Williams DS, Koretsky AP. Evidence for the exchange of arterial spin-labeled water with tissue water in rat brain from diffusion-sensitized measurements of perfusion. *Magn Reson Med* 1997;38(2):232.
- Wang J, Fernandez-Seara MA, Wang S, St Lawrence KS. When perfusion meets diffusion: in vivo measurement of water permeability in human brain. *J Cereb Blood Flow Metab* 2007;27(4):839–849.
- Ye FQ, Mattay VS, Jezzard P, Frank JA, Weinberger DR, McLaughlin AC. Correction for vascular artifacts in cerebral blood flow values measured by using arterial spin tagging techniques. *Magn Reson Med* 1997;37(2):226.
- Alsop DC, Detre JA. Reduced transit-time sensitivity in noninvasive magnetic resonance imaging of human cerebral blood flow. *J Cereb Blood Flow Metab* 1996;16(6):1236.
- Wang J, Alsop DC, Song HK, Maldjian JA, Tang K, Salvucci AE, Detre JA. Arterial transit time imaging with flow encoding arterial spin tagging (FEAST). *Magn Reson Med* 2003;50(3):599–607.
- Dai W, Garcia D, de Bazelaire C, Alsop DC. Continuous flow-driven inversion for arterial spin labeling using pulsed radio frequency and gradient fields. *Magn Reson Med* 2008;60(6):1488–1497.
- Wu WC, Fernandez-Seara M, Detre JA, Wehrli FW, Wang J. A theoretical and experimental investigation of the tagging efficiency of pseudocontinuous arterial spin labeling. *Magn Reson Med* 2007;58(5):1020–1027.
- Ye FQ, Frank JA, Weinberger DR, McLaughlin AC. Noise reduction in 3D perfusion imaging by attenuating the static signal in arterial spin tagging (ASSIST). *Magn Reson Med* 2000;44(1):92.
- St Lawrence KS, Frank JA, Bandettini PA, Ye FQ. Noise reduction in multi-slice arterial spin tagging imaging. *Magn Reson Med* 2005;53(3):735–738.
- Wang Z, Wang J, Connick TJ, Wetmore GS, Detre JA. Continuous ASL (CASL) perfusion MRI with an array coil and parallel imaging at 3T. *Magn Reson Med* 2005;54(3):732–737.
- Parkes LM, Tofts PS. Improved accuracy of human cerebral blood perfusion measurements using arterial spin labeling: accounting for capillary water permeability. *Magn Reson Med* 2002;48(1):27.
- Wang J, Wu W-C, Wang S, Fernandez-Seara M, St Lawrence K, Wolf RD. Diffusion-weighted perfusion MRI: Initial experience in application to brain tumor. *Proc Inter Soc Magn Reson Med* 2007;15:2974.
- Wong EC. Vessel Encoded Arterial Spin Labeling Using Pseudo-Continuous Tagging. In: Proceedings of the 14th Annual Meeting of ISMRM, Seattle, WA, USA, 2006 (Abstract 668).
- Dixon WT, Sardashti M, Castillo M, Stomp GP. Multiple inversion recovery reduces static tissue signal in angiograms. *Magn Reson Med* 1991;18(2):257–268.
- Pawlik G, Rackl A, Bing RJ. Quantitative capillary topography and blood flow in the cerebral cortex of cats: an in vivo microscopic study. *Brain Res* 1981;208(1):35.
- Kety SS. The theory and applications of the exchange of inert gas at the lungs and tissues. *Pharmacol Rev* 1951;3:1.
- Wang J, Alsop DC, Li L, Listerud J, Gonzalez-At JB, Schnall MD, Detre JA. Comparison of quantitative perfusion imaging using arterial spin labeling at 1.5 and 4.0 Tesla. *Magn Reson Med* 2002;48(2):242.
- Gelman N, Ewing JR, Gorell JM, Spickler EM, Solomon EG. Interregional variation of longitudinal relaxation rates in human brain at 3.0 T: relation to estimated iron and water contents. *Magn Reson Med* 2001;45(1):71–79.
- Asllani I, Borogovac A, Brown TR. Regression algorithm correcting for partial volume effects in arterial spin labeling MRI. *Magn Reson Med* 2008;60(6):1362–1371.
- Herscovitch P, Raichle ME, Kilbourn MR, Welch MJ. Positron emission tomographic measurement of cerebral blood flow and permeability-surface area product of water using [<sup>15</sup>O]water and [<sup>11</sup>C]butanol. *J Cereb Blood Flow Metab* 1987;7(5):527.

33. Eichling JO, Raichle ME, Grubb RL, Jr., Ter Pogossian MM. Evidence of the limitations of water as a freely diffusible tracer in brain of the rhesus monkey. *CircRes* 1974;35(3):358.
34. St Lawrence KS, Lee TY. An adiabatic approximation to the tissue homogeneity model for water exchange in the brain: II. Experimental validation. *J Cereb Blood Flow Metab* 1998;18(12):1378–1385.
35. Pardridge WM, Fierer G. Blood-brain barrier transport of butanol and water relative to N-isopropyl-p-iodoamphetamine as the internal reference. *J Cereb Blood Flow Metab* 1985;5(2):275–281.
36. Ginsberg MD, Busto R, Harik SI. Regional blood-brain barrier permeability to water and cerebral blood flow during status epilepticus: insensitivity to norepinephrine depletion. *Brain Res* 1985;337(1):59–71.
37. Larsson HB, Courivaud F, Rostrup E, Hansen AE. Measurement of brain perfusion, blood volume, and blood-brain barrier permeability, using dynamic contrast-enhanced T(1)-weighted MRI at 3 tesla. *Magn Reson Med* 2009;62(5):1270–1281.
38. Carr JP, Buckley DL, Tessier J, Parker GJ. What levels of precision are achievable for quantification of perfusion and capillary permeability surface area product using ASL? *Magn Reson Med* 2007;58(2):281–289.
39. Fernandez-Seara MA, Edlow BL, Hoang A, Wang J, Feinberg DA, Detre JA. Minimizing acquisition time of arterial spin labeling at 3T. *Magn Reson Med* 2008;59(6):1467–1471.
40. Zaharchuk G, Bogdanov AA, Jr., Marota JJ, Shimizu-Sasamata M, Weisskoff RM, Kwong KK, Jenkins BG, Weissleder R, Rosen BR. Continuous assessment of perfusion by tagging including volume and water extraction (CAPTIVE): a steady-state contrast agent technique for measuring blood flow, relative blood volume fraction, and the water extraction fraction. *Magn Reson Med* 1998;40(5):666.
41. Priya AK, Yan L, Wang DJ. Is cerebral microvascular flow anisotropic - preliminary evidence from multi-directional diffusion weighted perfusion MRI. *Proc Inter Soc Magn Reson Med* 2011;19:2114.